CrossMark

ARTICLE

Metal–Organic Framework-Assisted Synthesis of Compact Fe_2O_3 Nanotubes in Co_3O_4 Host with Enhanced Lithium Storage Properties
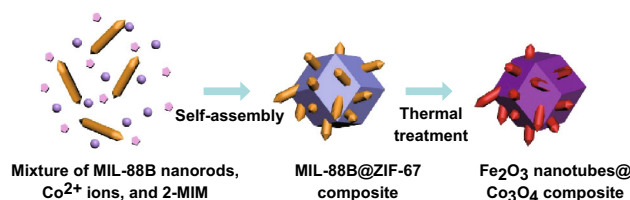
Song Lin Zhang[1] · Bu Yuan Guan[1] · Hao Bin Wu[2] · Xiong Wen David Lou[1]

Highlights

- A metal–organic framework (MOF)-assisted approach is developed for the synthesis of hierarchical composite particles composed of Fe_2O_3 nanotubes encapsulated in a Co_3O_4 host matrix.
- The hierarchical Fe_2O_3 nanotubes@Co_3O_4 composite particles exhibit excellent electrochemical performance when evaluated as an anode material for lithium-ion batteries (LIBs).

Abstract Transition metal oxides are promising candidates for the high-capacity anode material in lithium-ion batteries. The electrochemical performance of transition metal oxides can be improved by constructing suitable composite architectures. Herein, we demonstrate a metal–organic framework (MOF)-assisted strategy for the synthesis of a hierarchical hybrid nanostructure composed of Fe_2O_3 nanotubes assembled in Co_3O_4 host. Starting from MOF composite precursors (Fe-based MOF encapsulated in a Co-based host matrix), a complex structure of Co_3O_4 host and engulfed Fe_2O_3 nanotubes was prepared by a simple annealing treatment in air. By virtue of their structural and compositional features, these hierarchical composite particles reveal enhanced lithium storage properties when employed as anodes for lithium-ion batteries.

Mixture of MIL-88B nanorods, Co^{2+} ions, and 2-MIM → Self-assembly → MIL-88B@ZIF-67 composite → Thermal treatment → Fe_2O_3 nanotubes@ Co_3O_4 composite

✉ Bu Yuan Guan
guanbuyuan@ntu.edu.sg

✉ Xiong Wen David Lou
xwlou@ntu.edu.sg

1 School of Chemical and Biomedical Engineering, Nanyang Technological University, 62 Nanyang Drive, Singapore 637459, Singapore

2 School of Materials Science and Engineering, Zhejiang University, Hangzhou 310027, People's Republic of China

1 Introduction

Lithium-ion batteries (LIBs) have drawn considerable research attention as a rechargeable power source for portable electronic devices and electric vehicles [1, 2]. Until now, graphite has been the most commonly used anode material in commercial LIBs [3]. However, the relatively low theoretical capacity (372 mAh g^{-1}) of graphite is inadequate to meet the growing demands of energy density and life span in next-generation batteries [4–7].
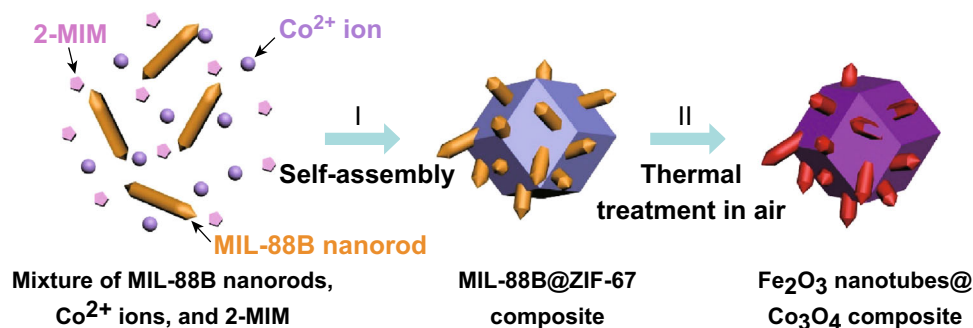
Fig. 1 Schematic illustration of the formation process of the Fe$_2$O$_3$ nanotubes@Co$_3$O$_4$ composite. (I) Self-assembly of MIL-88B nanorods, Co^{2+} ions, and 2-methylimidazole (2-MIM) to a MIL-88B@ZIF-67 composite. (II) Transformation to Fe$_2$O$_3$ nanotubes@Co$_3$O$_4$ composite through thermal treatment in air

Transition metal oxides (TMOs) have been considered as promising electrode materials for LIBs owing to their high specific capacity, low cost, and synthetic versatility to diverse nanostructures [8–11]. As two representative TMOs, iron oxide and cobalt oxide have been actively investigated [12–18]. However, the practical application of these anode materials still faces serious challenges, such as fast capacity fading, poor rate performance caused by large volume changes occurring during the lithiation/delithiation processes, and low intrinsic electric conductivity.

To overcome these drawbacks, diverse approaches have been proposed to improve the lithium storage properties. One effective way is to integrate two or more TMO materials into hybrid nanostructures [3, 19, 20]. The hybrid configuration is expected to retain the advantages of each component and, at the same time, provide synergetic effects that enhance the physicochemical properties such as electrochemical reactivity and mechanical stability [21]. Recently, several iron oxide@cobalt oxide hybrid materials have been reported with enhanced lithium storage capability, such as Fe$_2$O$_3$@Co$_3$O$_4$@C composite nanoparticles [22], Fe$_2$O$_3$@Co$_3$O$_4$ nanowire arrays [23], and Co$_3$O$_4$@Fe$_2$O$_3$ core–shell nanoneedle arrays [24]. In addition, the construction of hierarchical hollow nanostructures was found to be an effective way to accommodate the large volume changes associated with electrochemical reactions [25, 26]. The permeable shells can reduce Li$^+$ ion diffusion length and guarantee sufficient electrode–electrolyte contact area. Therefore, a rational design and synthesis approach for iron oxide@cobalt oxide hybrid electrodes with hierarchical hollow nanostructures is expected to yield enhanced lithium storage properties.

In recent years, there have been growing research interest for designing advanced electrode materials with controlled architectures and chemical compositions using metal–organic framework (MOF)-based precursors [27–35]. Most MOF-derived blends are based on simple MOF crystals, and the resulting nanomaterials exhibit relatively simple porous or hollow structures. A rational design of MOF hybrid precursors with novel structures and tailored compositions is highly desirable for the synthesis of high-performance electrode materials [36, 37].

In this work, we adopted a MOF-assisted approach for the synthesis of hierarchical composite particles of Fe$_2$O$_3$ nanotubes encapsulated in Co$_3$O$_4$ hosts for potential use as an anode material in LIBs. The strategy involves incorporation of MIL-88B (a Fe-based MOF) nanorods in a zeolitic imidazolate framework-67 (ZIF-67, a Co-based MOF) crystal. By a pyrolysis process, the hybrid precursor is transformed into compact Fe$_2$O$_3$ nanotubes engulfed within the Co$_3$O$_4$ host matrix (denoted as the Fe$_2$O$_3$ nanotubesCo$_3$O$_4$ composites) (Fig. 1). Benefiting from the unique structure and robust matrix, the as-prepared hierarchical Fe$_2$O$_3$ nanotubes@Co$_3$O$_4$ composite particles exhibit remarkable electrochemical performance when evaluated as an anode material for LIBs.

2 Experimental

2.1 Synthesis of MIL-88B@ZIF-67 Composites

The MIL-88B nanorods were synthesized by following a hydrothermal method reported earlier [38]. In this method, 0.16 g of F127 was first dissolved in 15 mL of deionized water to which 0.179 g of FeCl$_3$·6H$_2$O was added. The solution mixture was stirred for 1 h, and 0.6 mL of acetic acid was added to it. After stirring for 1 h, 0.06 g of 2-aminoterephthalic acid was injected. It was stirred for another 2 h, after which the reaction mixture was transferred into an autoclave and crystallized for 24 h at 110 °C. The resulting product was washed with ethanol several times. It was then dispersed with 10 mL of methanol solution containing 0.5 g of polyvinylpyrrolidone (PVP, M_w = 40,000), and the mixture was stirred at room temperature for 12 h. The PVP-functionalized MIL-88B nanorods were collected by centrifugation, washed several times with methanol, and dispersed in 15 mL of methanol for further use. To

synthesize the MIL-88B@ZIF-67 composite, 0.8 mL of the MIL-88B nanorod suspension, 5 mL of 80 mM 2-methylimidazole (2-MIM) solution, and 3 mL of 20 mM $Co(NO_3)_2 \cdot 6H_2O$ solution were mixed and allowed to react at room temperature for 4 h without stirring. The reaction product was extracted by centrifugation, washed with methanol several times, and vacuum-dried overnight.

2.2 Thermal Synthesis of Fe_2O_3 Nanotubes@Co_3O_4 Composites

The as-formed MIL-88B@ZIF-67 composite was placed in a ceramic boat and heated to 500 °C at a ramp rate of 5 °C min^{-1} in a tube furnace under ambient atmosphere. The temperature was maintained for 2 h after which the furnace was naturally cooled to room temperature.

2.3 Materials Characterization

Field-emission scanning electron microscope (FESEM; JEOL-6700F) and transmission electron microscope (TEM; JEOL-2010) were used to examine the morphology and structure of the prepared samples. The composition was analyzed by an energy-dispersive X-ray analysis (EDX) equipment attached to the FESEM instrument. The crystal phase was examined using a Bruker D2 Phaser X-ray diffractometer. Elemental mapping and high-angle annular dark-field scanning transmission

electron microscopy (HAADF-STEM) were performed in a JEOL-2100F electron microscope. Nitrogen sorption isotherms were measured using Autosorb 6B.

2.4 Electrochemical Measurements

Electrochemical measurements were carried out using CR2032 coin-type half cells. The working electrode consists of an active material (here, Fe_2O_3 nanotubes@Co_3O_4 composite particles), carbon black (Super-P–Li), and a polymer binder (polyvinylidene fluoride) in the weight ratio of 70:20:10. The loading mass of the active material is approximately 0.5–0.8 mg cm^{-2} for each electrode. Lithium foil was used for both the counter and reference electrodes. $LiPF_6$ (1.0 M) in a 50:50 (w/w) mixture of ethylene carbonate and diethyl carbonate was used as the electrolyte. The cell assembly was placed in an Ar-filled glove box with moisture and oxygen concentrations below 1.0 ppm. The galvanostatic charge–discharge tests were performed with a Neware battery test system.

3 Results and Discussion

MOF-based precursors have been widely used to fabricate inorganic functional materials with various micro-/nanostructures. To enable the synthesis of complex
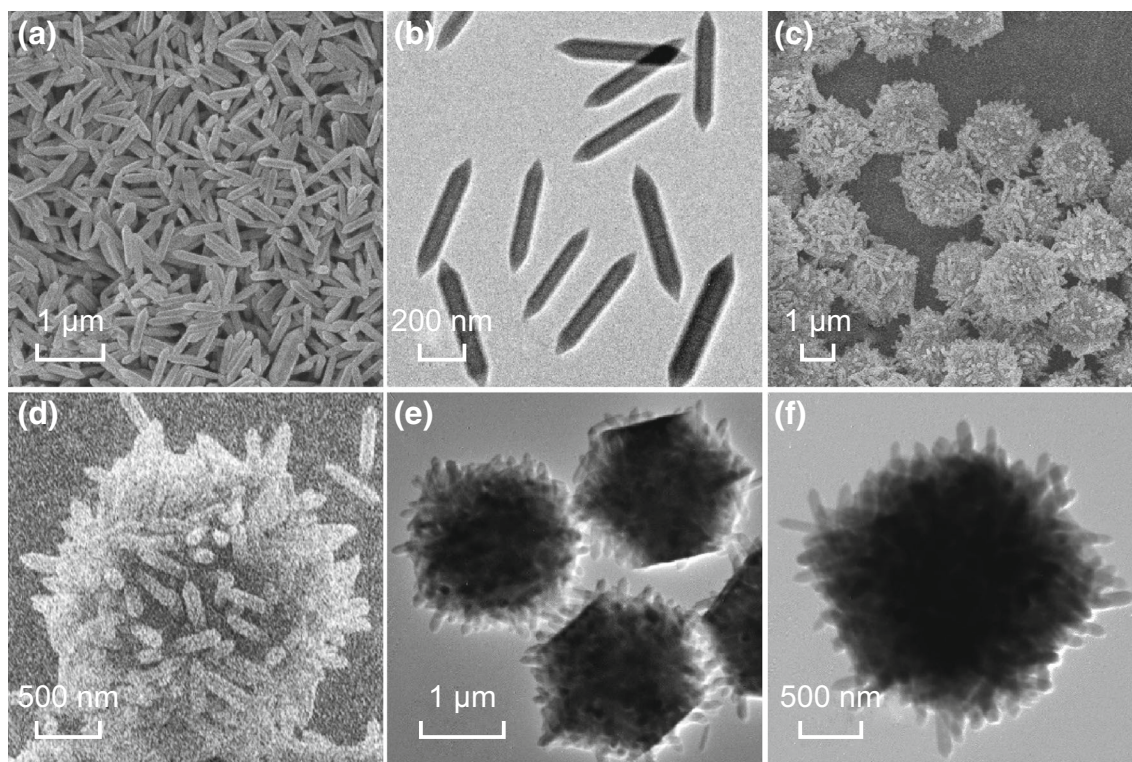

Fig. 2 FESEM images of **a** PVP-functionalized MIL-88B nanorods and **c, d** MIL-88B@ZIF-67 composites. TEM images of **b** PVP-functionalized MIL-88B nanorods and **e, f** MIL-88B@ZIF-67 composites

micro-/nanostructured materials, composite MOF precursors with multiple components are highly desirable, even though the synthesis is quite challenging [39, 40]. A facile solution-based method developed here easily facilitates the assembly of pre-synthesized MIL-88B nanorods within each ZIF-67 crystal. The MIL-88B nanorods synthesized through a modified hydrothermal method [38] are firstly functionalized with PVP on their surface (Fig. 2a, b). The incorporation of MIL-88B nanorods in the ZIF-67 crystal host was carried out by mixing MIL-88B nanorods with the

metal ions and organic ligands of ZIF-67 in methanol, and maintaining at room temperature for 4 h [41]. FESEM images show the morphology of the resulting composite particles (Fig. 2c, d). The uniform particles with a size of 2–3 μm exhibit a very rough surface composed of randomly oriented MIL-88B nanorods. TEM images further reveal the solid feature of each ZIF-67 crystal, with numerous MIL-88B nanorods uniformly distributed within each particle (Fig. 2e, f).

As seen in the XRD patterns (Fig. 3), the MIL-88B@ZIF-67 composites exhibit the diffraction peaks of both MIL-88B and ZIF-67 with high crystallinity. In addition, the successful incorporation of MIL-88B nanorods in ZIF-67 crystals can be visualized by the dark red color of the resultant product, which is quite different from the purple color of pristine ZIF-67 (insets of Fig. 3).

The Fe_2O_3 nanotubes@Co_3O_4 composites were synthesized by thermal treatment of MIL-88B@ZIF-67 precursors at 500 °C in air. Figure 4a shows a low-magnification FESEM image of the as-derived Fe_2O_3 nanotubes@Co_3O_4 composite particles. The composite sample preserves the morphology of its MOF precursor even after annealing treatment. A shrinkage of both rhombic dodecahedral hosts and rod-shaped guests is observed after the pyrolysis process, while the surface roughness of the annealed particles increased (Fig. 4b, c). The structure of the as-derived Fe_2O_3 nanotubes@Co_3O_4 composite was further examined
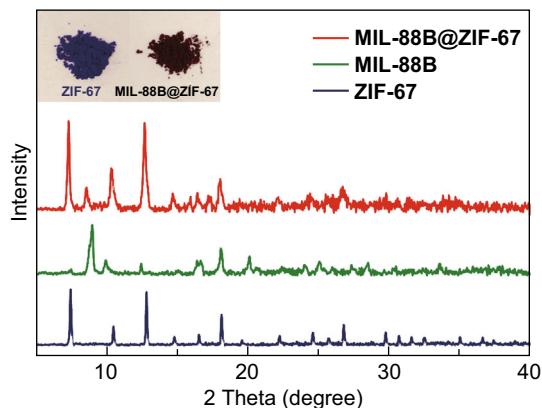
Fig. 3 XRD patterns of MIL-88B@ZIF-67 composites, MIL-88B and ZIF-67. Insets show the digital photographs of the MIL-88B@ZIF-67 composites and ZIF-67
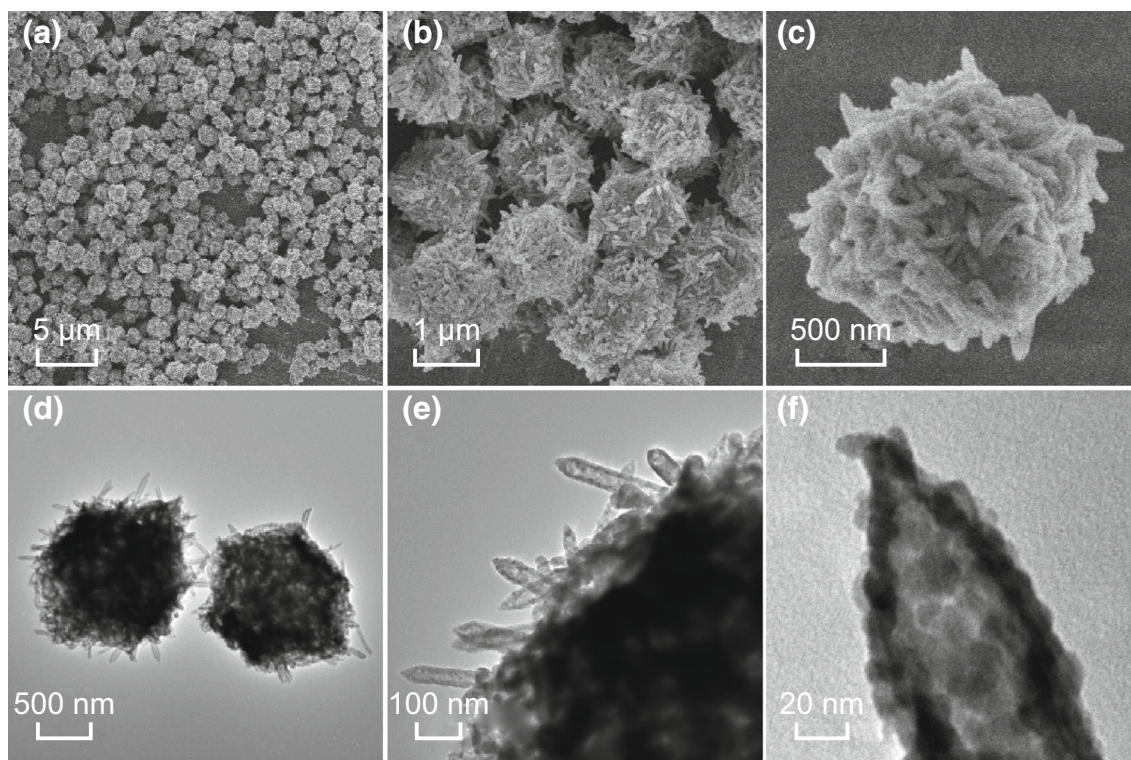
Fig. 4 **a–c** FESEM images and **d–f** TEM images of the Fe_2O_3 nanotubes@Co_3O_4 composites
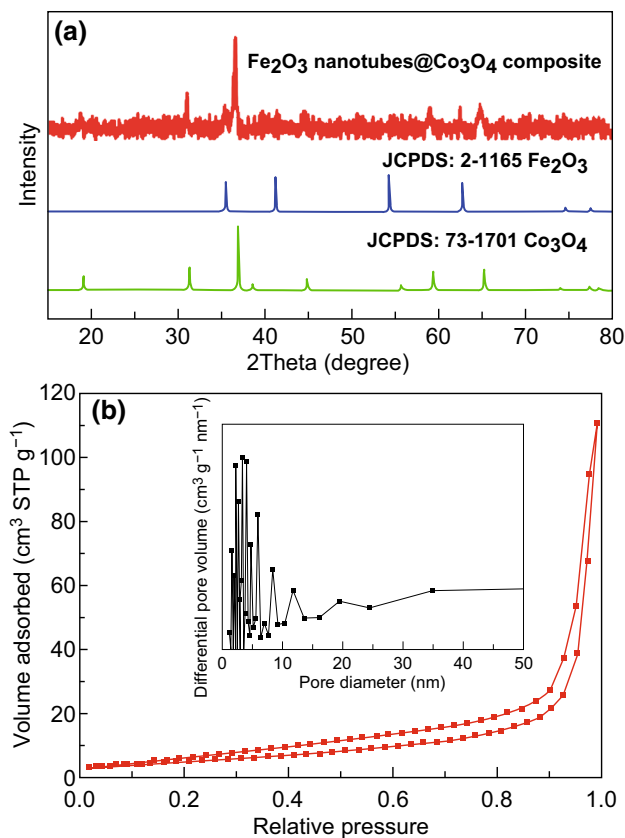
Fig. 5 a XRD pattern of the Fe_2O_3 nanotubes@Co_3O_4 composites. **b** N_2 sorption isotherms of the Fe_2O_3 nanotubes@Co_3O_4 composites. Inset gives the pore size distribution

by TEM. As shown in Fig. 4d, e, the Fe_2O_3 nanotubes derived from MIL-88B nanorods are evenly distributed in the Co_3O_4 host matrix. The length and diameter of the Fe_2O_3 nanotubes are about 455 and 55 nm, respectively (Fig. S1). A closer observation of the edge of a Fe_2O_3 nanotubes@Co_3O_4 composite particle reveals that each Fe_2O_3 nanotube is composed of small nanocrystallites (Fig. 4f). High-resolution TEM images (Fig. S2) confirm this observation, in which the lattice fringes assigned to the crystal planes of Fe_2O_3 and Co_3O_4 are clearly discernible.

The crystalline phases in the composite material were confirmed by powder XRD analysis (Fig. 5a). The XRD patterns were indexed to a mixture of δ-Fe_2O_3 phase (JCPDS card No. 2-1165) and cubic Co_3O_4 phase (JCPDS card No. 73-1701). The nitrogen sorption measurement indicates a moderate surface area of ∼ 18 m^2 g^{-1} for the Fe_2O_3 nanotubes@Co_3O_4 composite (Fig. 5b). Such a compact architecture may help to provide relatively good structural robustness and suppress parasitic side reactions between electrode and electrolyte [42, 43]. For comparison, Fe_2O_3 and Co_3O_4 nanostructures (derived from MIL-88B and ZIF-67) reveal Brunauer–Emmett–Teller (BET) surface areas of 7 and 45 m^2 g^{-1}, respectively (Fig. S3). From

an analysis of the chemical composition (by EDX), the Fe to Co molar ratio was obtained as 0.58:1 (Fig. S4). This value is very close to the experimental molar ratio (0.59:1) of Fe to Co that was used for synthesis. The spatial distribution of iron and cobalt oxides is shown in Fig. 6, as obtained from HAADF-STEM images and elemental mapping. The Fe_2O_3 nanotubes are seen to be evenly dispersed in the Co_3O_4 host matrix. X-ray photoelectron spectroscopy (XPS) measurements helped to identify the various valence states of Fe, Co, and O in the Fe_2O_3 nanotubes@Co_3O_4 composites (Fig. S5a). The binding energies of Fe $2p_{3/2}$ and $2p_{1/2}$ peaks are located at 707.8 and 721.3 eV, respectively, confirming the presence of Fe^{3+} state in Fe_2O_3 (Fig. S5b). The binding energies at 776.7 and 792.1 eV in the Co 2p spectrum are attributed to the Co^{2+} and Co^{3+} states in Co_3O_4 (Fig. S5c). The O 1 s spectrum can be deconvoluted into two bands at 284.4 and 285.1 eV, which are assigned to the O^{2-} state in Fe_2O_3 and Co_3O_4, respectively (Fig. S5d).

Subsequently, we evaluated the electrochemical lithium storage properties of Fe_2O_3 nanotubes@Co_3O_4 composite particles for use as an anode material in LIBs. Figure 7a shows the representative discharge–charge voltage profiles of Fe_2O_3 nanotubes@Co_3O_4 composite particles at a current density of 0.5 A g^{-1} within a cutoff voltage window of 0.01–3.0 V. The initial discharge and charge capacities are 921.9 and 709.8 mAh g^{-1}, respectively, with a high initial coulombic efficiency of 77.0%. The long discharge plateau at 0.84 V during the first cycle corresponds to the insertion of Li^+ ions into Fe_2O_3/Co_3O_4, complete reduction of Fe_2O_3/Co_3O_4 to metallic Fe/Co, and solid electrolyte interphase (SEI) film formation [22–24]. After the first cycle, the capacity becomes stable. Figure 7b shows the cycling performance of the Fe_2O_3 nanotubes@Co_3O_4 composite particles at a current density of 0.5 A g^{-1}. The capacity decays from the initial value of 922 to 710 mAh g^{-1} in the second cycle. Afterward, the capacity gradually increases to 951 mAh g^{-1} at the end of 80 cycles. The increase in capacity during cycling is commonly observed in many metal oxide-based anode materials [44, 45]. This phenomenon might be associated with the gradual activation of the Fe_2O_3@Co_3O_4 composite during cycling, which enhances the accessibility of lithium ions in the electrode material [46, 47]. The FESEM and TEM images of the Fe_2O_3 nanotubes@Co_3O_4 electrode after cycling are shown in Fig. S6. It is seen that the Fe_2O_3 nanotubes@Co_3O_4 composites retain their hierarchical structure even after 80 cycles. Few tubular subunits can still be observed on the edge of the hybrid particle. The cycling performance at a higher current density of 1.0 A g^{-1} is further testimony to the electrochemical stability of the hierarchical structure during the lithiation/delithiation processes (Fig. S7). For comparison, MIL-
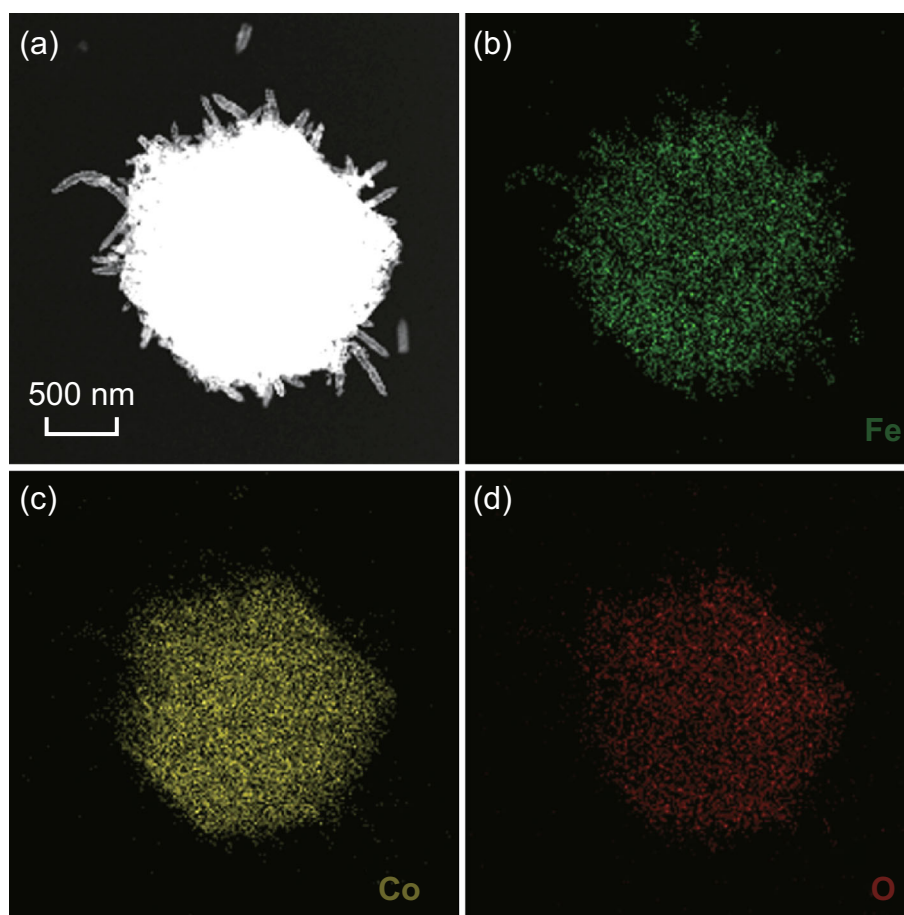
Fig. 6 **a** HAADF-STEM image of Fe_2O_3 nanotubes@Co_3O_4 composite particles. Elemental mapping images of **b** Fe, **c** Co, and **d** O

88B- and ZIF-67-derived Fe_2O_3 and Co_3O_4 nanostructures were also prepared by pyrolysis of the corresponding MOF precursors and studied. These exhibited inferior electrochemical stability (Fig. S8). Further, as shown in Fig. 7c, the Fe_2O_3 nanotubes@Co_3O_4 composite particles display good rate capability at discharge–charge current rates ranging from 0.1 to 2 A g^{-1}. The average specific capacities observed are 731, 717, 699, 628, and 554 mAh g^{-1} at current densities of 0.1, 0.2, 0.5, 1, and 2 A g^{-1}, respectively. After the high-rate discharge/charge cycling, a high specific capacity of 791 mAh g^{-1} was seen to be retained even when the current density returned to a low value of 0.1 A g^{-1}. To further investigate the mechanism of lithium storage in Fe_2O_3 nanotubes@Co_3O_4 composites, the cyclic voltammetry (CV) behavior of various cycles was investigated (Fig. S9). In the first cycle, cathodic peaks were observed at 1.72 and 0.40 V that correspond to the insertion of Li$^+$ into Fe_2O_3/Co_3O_4 and complete reduction of Fe_2O_3/Co_3O_4 to metallic Fe/Co, respectively [23]. The peaks at 1.70 and 2.13 V are ascribed to the delithiation processes and restoration of Fe_2O_3/Co_3O_4 [22, 24]. The subsequent curves show good reproducibility, with two

cathodic peaks at 0.69 and 1.30 V and two anodic peaks at 1.70 and 2.13 V. The conversion reaction of Fe_2O_3/Co_3O_4 with Li$^+$ is schematically illustrated (Fig. S10) to show the formation of metallic Fe/Co nanoparticles embedded in a matrix of Li_2O. These results demonstrate that the Fe_2O_3 nanotubes@Co_3O_4 composite particles possess excellent electrochemical kinetics and lithium storage characteristics comparable to many other Fe_2O_3, Co_3O_4, and their composites, which are useful for electrode materials, as reported previously (Table S1).

Overall, we regard that the outstanding lithium storage properties are attributable to a combination of the following factors. First, the assembly of compact Fe_2O_3 nanotubes in each Co_3O_4 host provides synergistic effects between two metal oxides with slightly different redox potentials [22–24]. This facilitates the electrochemical reactions and guarantees high energy density. Second, the hierarchical multilevel cavities and robust architecture lead to an increase in the electrode/electrolyte contact area and help to accommodate the strain of Li$^+$ insertion/extraction, hence contributing to good cycling stability. Finally, the nanosized subunits facilitate electronic/Li$^+$ transport in the
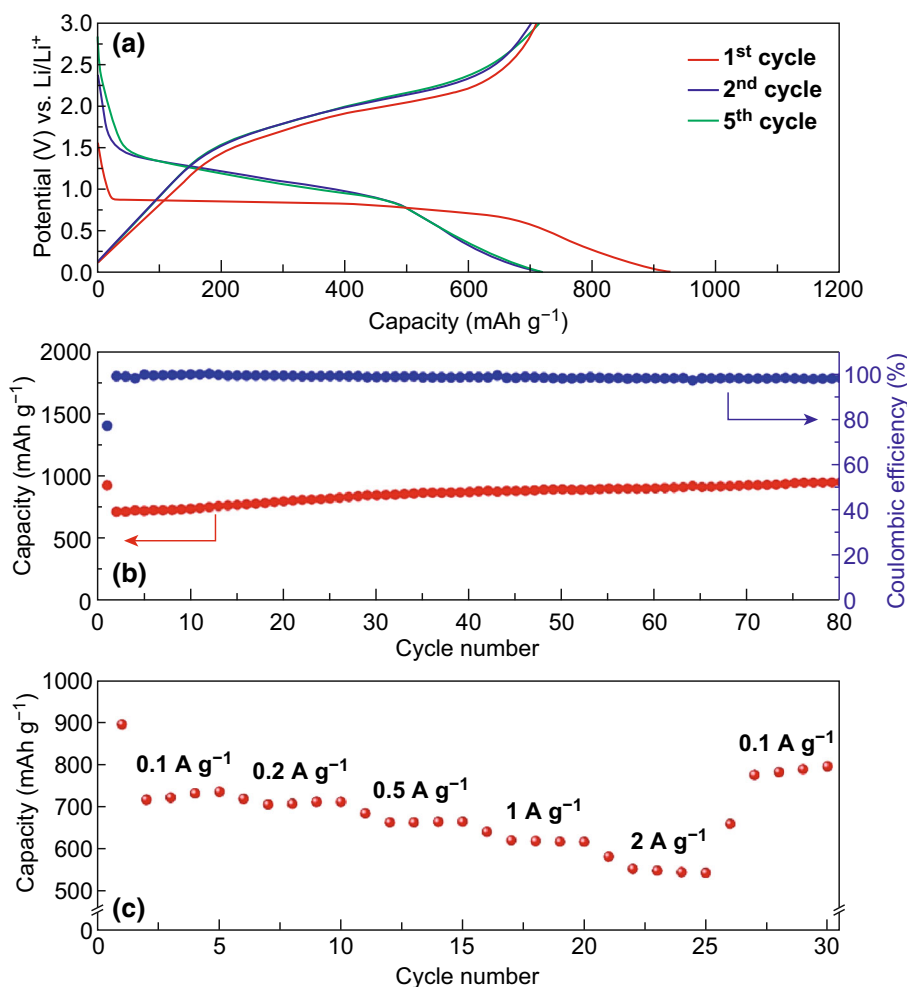
Fig. 7 Electrochemical characterization of the Fe_2O_3 nanotubes@Co_3O_4 composite as an anode material in LIBs. **a** Discharge–charge voltage profiles in the voltage range 0.01–3.0 V at a current density of 0.5 A g^{-1}. **b** Cycling performance and corresponding coulombic efficiency at a current density of 0.5 A g^{-1}. **c** Rate performance at various current densities from 0.1 to 2 A g^{-1}

electrode material, ensuring enhanced electrochemical activity. All of the above make the Fe_2O_3 nanotubes@Co_3O_4 composite particles a highly promising anode material for LIBs.

4 Conclusion

A novel MOF-assisted strategy has been developed to construct a complex hierarchical nanostructure consisting of compact Fe_2O_3 nanotubes encapsulated in Co_3O_4 host. The synthesis involves incorporation of MIL-88B nanorods in the ZIF-67 polyhedron host followed by a thermal treatment process in air to convert the MIL-88B nanorods and ZIF-67 polyhedron to Fe_2O_3 nanotubes and Co_3O_4 host, respectively. Benefiting from the unique structural and compositional advantages, the as-prepared hierarchical Fe_2O_3 nanotubes@Co_3O_4 composite exhibits outstanding electrochemical properties with good rate

capability and excellent cycling stability as an anode material for LIBs. Our study sheds new light on the controlled synthesis of complex hollow structures for various energy-related applications.

References

1. J.M. Tarascon, M. Armand, Issues and challenges facing rechargeable lithium batteries. Nature **414**, 359–367 (2001). https://doi.org/10.1038/35104644

2. B. Dunn, H. Kamath, J.-M. Tarascon, Electrical energy storage for the grid: a battery of choices. Science **334**(6058), 928–935 (2011). https://doi.org/10.1126/science.1212741

3. X.-B. Cheng, R. Zhang, C.-Z. Zhao, Q. Zhang, Toward safe lithium metal anode in rechargeable batteries: a review. Chem. Rev. **117**(15), 10403–10473 (2017). https://doi.org/10.1021/acs.chemrev.7b00115

4. M. Winter, R.J. Brodd, What are batteries, fuel cells, and supercapacitors? Chem. Rev. **104**(10), 4245–4270 (2004). https://doi.org/10.1021/cr020730k

5. P. Meduri, E. Clark, E. Dayalan, G.U. Sumanasekera, M.K. Sunkara, Kinetically limited de-lithiation behavior of nanoscale tin-covered tin oxide nanowires. Energy Environ. Sci. **4**(5), 1695–1699 (2011). https://doi.org/10.1039/C1EE01041G

6. J.B. Goodenough, K.-S. Park, The Li-ion rechargeable battery: a perspective. J. Am. Chem. Soc. **135**(4), 1167–1176 (2013). https://doi.org/10.1021/ja3091438

7. L. Lin, X. Xu, C. Chu, M.K. Majeed, J. Yang, Mesoporous amorphous silicon: a simple synthesis of a high-rate and long-life anode material for lithium-ion batteries. Angew. Chem. Int. Ed. **55**(45), 14063–14066 (2016). https://doi.org/10.1002/anie.201608146

8. X.W. Lou, L.A. Archer, Z. Yang, Hollow micro-/nanostructures: synthesis and applications. Adv. Mater. **20**(21), 3987–4019 (2008). https://doi.org/10.1002/adma.200800854

9. B.Y. Guan, L. Yu, J. Li, X.W. Lou, A universal cooperative assembly-directed method for coating of mesoporous TiO₂ nanoshells with enhanced lithium storage properties. Sci. Adv. **2**(3), e1501554 (2016). https://doi.org/10.1126/sciadv.1501554

10. H. Ren, R. Yu, J. Wang, Q. Jin, M. Yang, D. Mao, D. Kisailus, H. Zhao, D. Wang, Multishelled TiO₂ hollow microspheres as anodes with superior reversible capacity for lithium ion batteries. Nano Lett. **14**(11), 6679–6684 (2014). https://doi.org/10.1021/nl503378a

11. B.Y. Guan, X.Y. Yu, H.B. Wu, X.W. Lou, Complex nanostructures from materials based on metal–organic frameworks for electrochemical energy storage and conversion. Adv. Mater. **29**(47), 1703614 (2017). https://doi.org/10.1002/adma.201703614

12. L. Zhang, H.B. Wu, S. Madhavi, H.H. Hng, X.W. Lou, Formation of Fe₂O₃ microboxes with hierarchical shell structures from metal–organic frameworks and their lithium storage properties. J. Am. Chem. Soc. **134**(42), 17388–17391 (2012). https://doi.org/10.1021/ja307475c

13. J. Wang, N. Yang, H. Tang, Z. Dong, Q. Jin et al., Accurate control of multishelled Co₃O₄ hollow microspheres as high-performance anode materials in lithium-ion batteries. Angew. Chem. Int. Ed. **52**(25), 6417–6420 (2013). https://doi.org/10.1002/anie.201301622

14. F.-X. Ma, H. Hu, H.B. Wu, C.-Y. Xu, Z. Xu, L. Zhen, X.W. Lou, Formation of uniform Fe₃O₄ hollow spheres organized by ultra-thin nanosheets and their excellent lithium storage properties. Adv. Mater. **27**(27), 4097–4101 (2015). https://doi.org/10.1002/adma.201501130

15. Y. Li, B. Tan, Y. Wu, Mesoporous Co₃O₄ nanowire arrays for lithium ion batteries with high capacity and rate capability. Nano Lett. **8**(1), 265–270 (2008). https://doi.org/10.1021/nl0725906

16. Y.M. Chen, L. Yu, X.W. Lou, Hierarchical tubular structures composed of Co₃O₄ hollow nanoparticles and carbon nanotubes for lithium storage. Angew. Chem. Int. Ed. **55**(20), 5990–5993 (2016). https://doi.org/10.1002/anie.201600133

17. C. He, S. Wu, N. Zhao, C. Shi, E. Liu, J. Li, Carbon-encapsulated Fe₃O₄ nanoparticles as a high-rate lithium ion battery anode material. ACS Nano **7**(5), 4459–4469 (2013). https://doi.org/10.1021/nn401059h

18. W.Y. Li, L.N. Xu, J. Chen, Co₃O₄ nanomaterials in lithium-ion batteries and gas sensors. Adv. Funct. Mater. **15**(5), 851–857 (2005). https://doi.org/10.1002/adfm.200400429

19. C. Wang, L. Wu, H. Wang, W. Zuo, Y. Li, J. Liu, Fabrication and shell optimization of synergistic TiO₂–MoO₃ core–shell nanowire array anode for high energy and power density lithium-ion batteries. Adv. Funct. Mater. **25**(23), 3524–3533 (2015). https://doi.org/10.1002/adfm.201500634

20. L. Yu, H. Hu, H.B. Wu, X.W. Lou, Complex hollow nanostructures: synthesis and energy-related applications. Adv. Mater. **29**(15), 1604563 (2017). https://doi.org/10.1002/adma.201604563

21. S. Wang, B.Y. Guan, L. Yu, X.W. Lou, Rational design of three-layered TiO₂@carbon@MoS₂ hierarchical nanotubes for enhanced lithium storage. Adv. Mater. **29**(37), 1702724 (2017). https://doi.org/10.1002/adma.201702724

22. I. Sultana, M.M. Rahman, T. Ramireddy, N. Sharma, D. Poddar, A. Khalid, H. Zhang, Y. Chen, A.M. Glushenkov, Understanding structure–function relationship in hybrid Co₃O₄–Fe₂O₃/C lithium-ion battery electrodes. ACS Appl. Mater. Interfaces. **7**(37), 20736–20744 (2015). https://doi.org/10.1021/acsami.5b05658

23. Q.Q. Xiong, X.H. Xia, J.P. Tu, J. Chen, Y.Q. Zhang, D. Zhou, C.D. Gu, X.L. Wang, Hierarchical Fe₂O₃@Co₃O₄ nanowire array anode for high-performance lithium-ion batteries. J. Power Sour. **240**(15), 344–350 (2013). https://doi.org/10.1016/j.jpowsour.2013.04.042

24. Y. Luo, D. Kong, J. Luo, Y. Wang, D. Zhang, K. Qiu, C. Cheng, C.M. Li, T. Yu, Seed-assisted synthesis of Co₃O₄@Fe₂O₃ core-shell nanoneedle arrays for lithium-ion battery anode with high capacity. RSC Adv. **4**(26), 13241–13249 (2014). https://doi.org/10.1039/C3RA47189F

25. B.Y. Guan, A. Kushima, L. Yu, S. Li, J. Li, X.W. Lou, Coordination polymers derived general synthesis of multishelled mixed metal-oxide particles for hybrid supercapacitors. Adv. Mater. **29**(17), 1605902 (2017). https://doi.org/10.1002/adma.201605902

26. L. Yu, J.F. Yang, X.W. Lou, Formation of CoS₂ nanobubble hollow prisms for highly reversible lithium storage. Angew. Chem. Int. Ed. **55**(43), 13422–13426 (2016). https://doi.org/10.1002/anie.201606776

27. H.B. Wu, S. Wei, L. Zhang, R. Xu, H.H. Hng, X.W. Lou, Embedding sulfur in MOF-derived microporous carbon polyhedrons for lithium–sulfur batteries. Chem.: Eur. J. **19**(33), 10804–10808 (2013). https://doi.org/10.1002/chem.201301689

28. K. Xi, S. Cao, X. Peng, C. Ducati, R. Vasant Kumar, A.K. Cheetham, Carbon with hierarchical pores from carbonized metal–organic frameworks for lithium sulphur batteries. Chem. Commun. **49**(22), 2192–2194 (2013). https://doi.org/10.1039/C3CC38009B

29. Y. Wang, X. Guo, Z. Wang, M. Lu, B. Wu, Y. Wang, C. Yan, A. Yuan, H. Yang, Controlled pyrolysis of MIL-88A to Fe₂O₃@C nanocomposites with varied morphologies and phases for advanced lithium storage. J. Mater. Chem. A **5**(48), 25562–25573 (2017). https://doi.org/10.1039/C7TA08314A

30. K. Zhang, H. Yang, M. Lü, C. Yan, H. Wu, A. Yuan, S. Lin, Porous MoO₂-Cu/C/graphene nano-octahedrons quadruple nanocomposites as an advanced anode for lithium ion batteries with enhanced rate capability. J. Alloys Compd. **731**, 646–654 (2018). https://doi.org/10.1016/j.jallcom.2017.10.091

31. Y. Chen, Y. Wang, H. Yang, H. Gan, X. Cai, X. Guo, B. Xu, M. Lü, A. Yuan, Facile synthesis of porous hollow Co₃O₄ microfibers derived-from metal–organic frameworks as an advanced anode for lithium ion batteries. Ceram. Int. **43**(13), 9945–9950 (2017). https://doi.org/10.1016/j.ceramint.2017.05.004

32. M. Sun, M. Sun, H. Yang, W. Song, Y. Nie, S. Sun, Porous Fe_2O_3 nanotubes as advanced anode for high performance lithium ion batteries. Ceram. Int. **43**(1), 363–367 (2017). https://doi.org/10.1016/j.ceramint.2016.09.166

33. B.Y. Guan, L. Yu, X.W. Lou, General synthesis of multishell mixed-metal oxyphosphide particles with enhanced electrocatalytic activity in the oxygen evolution reaction. Angew. Chem. Int. Edit. **56**(9), 2386–2389 (2017). https://doi.org/10.1002/anie.201611804

34. B.Y. Guan, L. Yu, X. Wang, S. Song, X.W. Lou, Formation of onion-like $NiCo_2S_4$ particles via sequential ion-exchange for hybrid supercapacitors. Adv. Mater. **29**(6), 1605051 (2017). https://doi.org/10.1002/adma.201605051

35. B.Y. Guan, L. Yu, X.W. Lou, A dual-metal–organic-framework derived electrocatalyst for oxygen reduction. Energy Environ. Sci. **9**(10), 3092–3096 (2016). https://doi.org/10.1039/C6EE02171A

36. B.Y. Guan, Y. Lu, Y. Wang, M. Wu, X.W. Lou, Porous iron–cobalt alloy/nitrogen-doped carbon cages synthesized via pyrolysis of complex metal–organic framework hybrids for oxygen reduction. Adv. Funct. Mater. **28**(10), 1706738 (2018). https://doi.org/10.1002/adfm.201706738

37. B.Y. Guan, L. Yu, X.W. Lou, Formation of single-holed cobalt/N-doped carbon hollow particles with enhanced electrocatalytic activity toward oxygen reduction reaction in alkaline media. Adv. Sci. **4**(10), 1700247 (2017). https://doi.org/10.1002/advs.201700247

38. S. Zhao, H. Yin, L. Du, L. He, K. Zhao et al., Carbonized nanoscale metal–organic frameworks as high performance electrocatalyst for oxygen reduction reaction. ACS Nano **8**(12), 12660–12668 (2014). https://doi.org/10.1021/nn505582e

39. H.B. Wu, X.W. Lou, Metal–organic frameworks and their derived materials for electrochemical energy storage and conversion: promises and challenges. Sci. Adv. **3**(12), eaap9252 (2017). https://doi.org/10.1126/sciadv.aap9252

40. H. Zhang, J. Nai, L. Yu, X.W. Lou, Metal–organic-framework-based materials as platforms for renewable energy and environmental applications. Joule **1**(1), 77–107 (2017). https://doi.org/10.1016/j.joule.2017.08.008

41. B.Y. Guan, X.W. Lou, Complex cobalt sulfide nanobubble cages with enhanced electrochemical properties. Small Methods **1**(7), 1700158 (2017). https://doi.org/10.1002/smtd.201700158

42. N. Liu, Z. Lu, J. Zhao, M.T. McDowell, H.-W. Lee, W. Zhao, Y. Cui, A pomegranate-inspired nanoscale design for large-volume-change lithium battery anodes. Nat. Nanotechnol. **9**, 187–192 (2014). https://doi.org/10.1038/nnano.2014.6

43. Z. Li, B.Y. Guan, J. Zhang, X.W. Lou, A compact nanoconfined sulfur cathode for high-performance lithium-sulfur batteries. Joule **1**(3), 576–587 (2017). https://doi.org/10.1016/j.joule.2017.06.003

44. F. Wu, C. Yu, W. Liu, T. Wang, J. Feng, S. Xiong, Large-scale synthesis of $Co_2V_2O_7$ hexagonal microplatelets under ambient conditions for highly reversible lithium storage. J. Mater. Chem. A **3**(32), 16728–16736 (2015). https://doi.org/10.1039/C5TA03106K

45. N. Yan, L. Hu, Y. Li, Y. Wang, H. Zhong, X. Hu, X. Kong, Q. Chen, Co_3O_4 nanocages for high-performance anode material in lithium-ion batteries. J. Phys. Chem. C **116**(12), 7227–7235 (2012). https://doi.org/10.1021/jp2126009

46. L. Xia, S. Wang, G. Liu, L. Ding, D. Li, H. Wang, S. Qiao, Flexible SnO_2/N-doped carbon nanofiber films as integrated electrodes for lithium-ion batteries with superior rate capacity and long cycle life. Small **12**(7), 853–859 (2016). https://doi.org/10.1002/smll.201503315

47. Y. Jiang, Z.-J. Jiang, L. Yang, S. Cheng, M. Liu, A high-performance anode for lithium ion batteries: Fe_3O_4 microspheres encapsulated in hollow graphene shells. J. Mater. Chem. A **3**(22), 11847–11856 (2015). https://doi.org/10.1039/C5TA01848J